Materials Research Proceedings 41 (2024) 1277-1287 https://doi.org/10.21741/9781644903131-142

Effect of micro-plasto-hydrodynamic lubrication on strip surface in steel cold rolling

ELHAJJ Cynthia[1,2,a *], LAHOUIJ Imène[1], LUONG Linh Phuong[2] and MONTMITONNET Pierre[1]

[1]Centre de Mise en Forme de Matériaux, MINES Paris | PSL Research University, CNRS UMR7635, France

[2]R&D research center, Aperam Stainless Europe, France

[a]cynthia.elhajj@minesparis.psl.eu

Keywords: MPHDL Lubrication, Numerical Modelling, Steel Cold Rolling, Surface Finish

Abstract. This study employs numerical calculations based on the micro-plasto-hydrodynamic lubrication (MPHDL) theory to analyze the evolution of oil pits during the stainless-steel cold rolling process. The model is enhanced by incorporating lubricant temperature variations caused by its contact with the heated roll and strip, as well as variations in pit slope. The findings show the significant impact and relevance of considering these additional parameters in assessing the performance of the MPHDL mechanism. Notably, the model demonstrates good agreement with experimental measurements conducted on a Stainless-Steel grade undergoing multiple passes.

Introduction

Controlling friction in Stainless Steel (SS) cold rolling leads to a better surface finish resulting in superior product quality and more favorable economic outcomes, to reduced roll load (smaller tooling deformation, hence easier strip profile and flatness control) and torque (reduced power required from motors). In cold rolling, prioritizing lubrication modeling is a fundamental factor to address the challenging notion of effective friction control. Nonetheless, it is crucial to note that lubrication involves two distinct subproblems [1]: global lubrication, involving the feeding of lubricant to the process entry point, and local micro-scale lubrication, diving into the interactions unfolding at the local scale of asperity.

Hot-rolled stainless steel, ready for cold rolling, is first subjected to shot-blasting and pickling operations. The sheets are therefore left with craters (Fig. 1) which must be smoothed out during cold rolling to obtain a bright, glossy surface finish. But they form oil pits which resist smoothing [2], compromising the gloss of high-quality stainless-steel products. This emphasizes the significance of a microscale lubrication mechanism that facilitates both pit closure, particularly focusing on its impact at the local (pit) scale. The pits (diameter ~80-100µm, depth ~10-20µm) form oil reservoirs. Due to macroscopic plastic deformation of the strip, as the free volumes between the strip and the roll surface is reduced, the lubricant is pressurized in the pits. At a certain point, due to a hydrodynamic effect, the lubricant will escape to form a micro-film (< 3 µm thick) on the adjacent plateau, a 2-scale lubrication mechanism. This promotes a relation between the asperity crushing rate (reduction of the pits) and the quantity of escaping lubricant from the micro-pits. This mechanism is called Micro Plasto-Hydro-Dynamic Lubrication (MPHDL) [3].

A lot of experimental and numerical work has been done on the MPHDL mechanism. Bech et al. [4] conducted experiments using a transparent tool in a strip drawing configuration. As they observed and confirmed the escape phenomenon of the lubricant, the more important revelation was the demonstration of the influence of various parameters on the tendency for either backward or forward escape (it was also more developed by Bay et al. [5]). Due to this escape, Ahmed and Sutcliffe [6] were interested to observe the reduction of pit under this mechanism in SS strip

drawing and cold rolling. They also established experimental method, using a three-dimensional profilometry data, to identify pits using different criteria [7]. In the same area, Sutcliffe and Georgiades [8] characterized and determined the pit features : depth, diameter and slope. The forward (HydroStatic, MPHSL) escape was addressed numerically as a cavity problem using a finite element method with a Darcy interfacial medium, following the model developed by Stephany et al. [9] and Caretta et al. [10]. The backward (HydroDynamic, MPHDL) escape was treated by Lo and Wilson[11] who assumed a workpiece consisting of triangular asperities transverse to the forming direction, compressed by a smooth tool ; they set up equations coupling strip plastic deformation, lubricant extraction and pit closure. Sutcliffe et al. [12] applied Lo and Wilson theory for a SS strip rolling and drawing case.

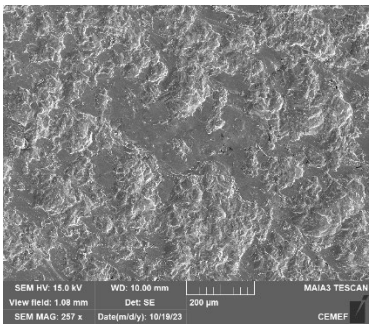

Fig. 1 Scanning Electron Microscope (SEM) observation of a stainless-steel strip surface subjected to shot blast and pickling.

This paper considers only MPHDL permeation without consideration of MPHSL or the global Plasto hydrodynamic lubrication (PHL). Its purpose is to rely on the methodology of Lo and Wilson model, incorporating additional parameters such as the effect of temperature or the pit slope variation, which have not been addressed previously, and assessing their impact on the effectiveness of this mechanism after a few passes.

Model Description

The purpose of this model is to show the influence of pit oil escape (quantified by h_1, the oil film thickness formed at the edge of an asperity) on the evolution of pit closure (quantified by $(1-A)$, where A is the actual contact area). Thus, the main idea is to find equations linking h_1 and A.

Asperity crushing: Studies have shown that asperities on the surface of the strip are crushed and flattened progressively while the strip is plastically deforming under the action of rolling, showing the influence of the macroscopic strain ε . At the same time, the asperity is locally deforming with its own strain ε_a and strain rate (extension rate) $\dot{\varepsilon}_a$ considered uniform and distinct from the strip elongation rate $\dot{\varepsilon}$ (the difference is due to the flattening, so that $\dot{\varepsilon}_a > \dot{\varepsilon}$). Mathematically, both macroscopic and microscopic deformation can be shown by expressing the asperity crushing velocity v_f using the time derivative of the mean depth of the asperity.

Fig. 2 shows the schematic of a triangular asperity. The geometry is described by the actual contact area A, the length between two consecutive asperities (the period) L and the slope of the asperity θ. In the present paper, the latter is allowed to vary, contrary to previous models of the literature. Considering small asperity slope θ, the depth of the asperity can be expressed as:

$$\delta = \frac{(1-A)L\theta}{2} \quad (1)$$

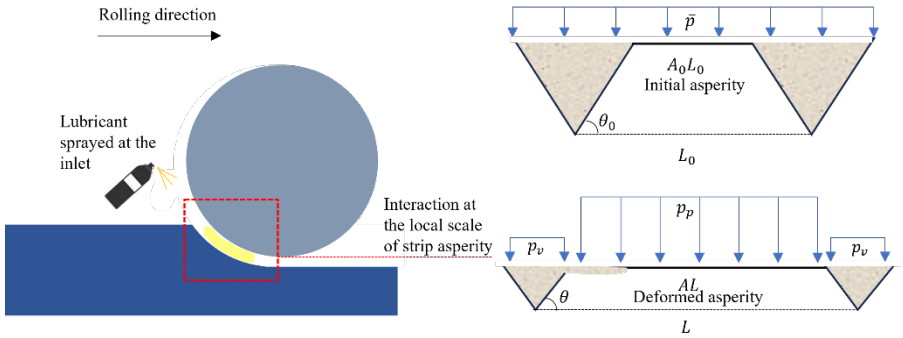

Fig. 2 Schematic of flattening of asperity with lubricant escape at the edge of the pit.

Before deriving, A and L are replaced in Eq.(1) using their expression in Appendix, thus the asperity crushing velocity (Fig. 11) $v_f = -\frac{1}{2}\frac{d\bar{\delta}}{dt}$, becomes:

$$v_f = -\frac{\theta L(\dot{\varepsilon}-A\dot{\varepsilon}_a)}{4} - \frac{\dot{\theta}(1-A)L}{4} \tag{2}$$

Where $\dot{\theta}$ is the asperity slope variation rate.

The local dimensionless crushing rate W is then defined for a better representation of the flattening process:

$$W = \frac{2v_f}{\dot{\varepsilon}L} \tag{3}$$

Combining Eq.(2) and Eq.(3) gives:

$$W = -\frac{\theta(\dot{\varepsilon}-A\dot{\varepsilon}_a)}{2\dot{\varepsilon}} - \frac{\dot{\theta}(1-A)}{2\dot{\varepsilon}} \tag{4}$$

A few hardness models [13,14,15,16] have been established to express the crushing rate function of the area of contact and the effective hardness $\Delta = \frac{p_p - p_v}{Y}$, where Y is the plane strain yield stress of the strip metal. The aim of those model is to compute the evolution of plateau and valley pressure respectively p_p and p_v. Between those models, we select Sutcliffe [17] correlation, thus W can be expressed as:

$$W = A(1-A)(C_1(\Delta) + C_2(\Delta)A + C_3(\Delta)A^2) \tag{5}$$

Where C_1, C_2 and C_3 are functions of Δ [17].

The plateau and valley pressure can be expressed as:

$$p_p = \bar{p} + (1-A)Y\Delta \tag{6}$$

$$p_v = \bar{p} - AY\Delta \tag{7}$$

In the previous equations $A = f(\dot{\varepsilon_a})$, so the only unknowns are $\dot{\varepsilon}_a$ and Δ. Combining Eq.(4) and Eq.(5) gives the first nonlinear equations in the system to solve. The second equation is derived in the next subsection. It describes the relation between the thickness h_1 of the oil film escaping through the edge of the pit, the asperity strain rate $\dot{\varepsilon}_a$ and effective hardness Δ.

Materials Research Proceedings 41 (2024) 1277-1287 https://doi.org/10.21741/9781644903131-142

Flow of lubricant escaping the pits: In this process, pits function as oil reservoirs. So, using Fig. 2, the oil volume in the triangle pit per unit width is defined as:

$$v = \frac{\delta^2}{2\theta} = \frac{\theta L^2 (1-A)^2}{4} \tag{8}$$

The fluid is assumed incompressible. Consider the control volume "lubricant + edge of the pit," the lubricant exits with a mean velocity $\bar{u}_1$expressed in Appendix while the edge of the pit is moving in accordance with the asperity deformation rate $\dot{\varepsilon_a}$. Using the conservation of mass, the mass flow of the lubricant exiting the reservoir is equal to the volume change in the reservoir per unit time. Differentiating Eq.(8) with respect to time gives:

$$\frac{dv}{dt} = \frac{\theta L^2 (1-A)(\dot{\varepsilon} - A\dot{\varepsilon_a})}{2} + \frac{\dot{\theta} L^2 (1-A)^2}{4} = -h_1 \left(\frac{\bar{u}_1 + \frac{AL\dot{\varepsilon_a}}{2}}{2} \right) \tag{9}$$

Arranging Eq.(9) gives a first expression of the oil film thickness, based on geometrical arguments:

$$h_1 = -\frac{2\theta L^2 (1-A)(\dot{\varepsilon} - A\dot{\varepsilon_a})}{2\bar{u}_1 + AL\dot{\varepsilon_a}} - \frac{\dot{\theta} L^2 (1-A)^2}{2\bar{u}_1 + AL\dot{\varepsilon_a}} \tag{10}$$

Note that in Eq.(4) and Eq.(10), if we consider the slope of the asperity unchanged during the stretching of the asperity (so that $\dot{\theta} = 0$) as in former approaches, Lo and Wilson equations are retrieved [11].

At this stage, h_1 is a function of $\dot{\varepsilon_a}$: we need a second equation which will be found using another expression of h_1.

Pressure distribution using Reynolds equation: The surface is subjected to a mean pressure $\bar{p}$ resulting in the reduction of the pit volume. The latter will be pressurized to the point of escape due to hydrodynamic action. This will change the redistribution of the pressure map; notice in Fig. 2 how the pressure on the plateau becomes higher than the mean pressure while in the valley it decreases below it. This redistribution can be determined solving the Reynolds equation. Thus, the 1-D simplified Reynolds equations for an incompressible fluid is given by:

$$\frac{dQ}{dh} = -\frac{12\eta[p(x),T(x)]\alpha\bar{u}_1}{\theta}\frac{h-h_0}{h^3} = -\frac{12\eta_0[T(x)]\alpha\bar{u}_1}{\theta}\frac{h-h_0}{h^3} \tag{11}$$

Where $Q = 1 - e^{-\alpha p}$ is the reduced pressure, α is the pressure viscosity coefficient and h_0 is a constant, the (unknown at this stage) thickness at the point where the pressure gradient becomes zero. The viscosity of the lubricant η is always taken in such models as a function of the pressure only, neglecting the temperature effect, e.g. $\eta = \eta_0 e^{\alpha p}$. However, in a steady cold rolling state, the roll and strip surface can be heated up to 200°C which will logically affect the temperature of the lubricant in contact with both surfaces and hence its viscosity. For this reason, the viscosity in the present model will be expressed as [18]:

$$\eta = \eta_0 e^{-\beta(T_{lub} - T_0)} \tag{12}$$

Where β is the temperature viscosity coefficient, $T_{lub} = \frac{T_{r,b} + T_{s,b}}{2}$ is the lubricant local temperature (where r stands for roll, s for strip and b for bite region) and T_0 is the temperature at which the viscosity η_0 is given (often 40°C). The expression of the viscosity can now be replaced

in Eq.(11). Integrating Eq.(11) with respect to h gives $Q = f(h) + Q_0$. The film thickness h_1 is considered small in front of the film thickness in the pit (equal to the depth of the pit), so that the pressure gradient becomes zero at the edge of the valley, resulting in $h_0 = h_1$. The boundary conditions are expressed as:

- At $h_1 = 0$, $Q_0 = 1 - e^{-\alpha p_v}$
- At $h = h_1 \neq 0, Q = 1 - e^{-\alpha p_p} = f(h_1) + Q_0$

The expression of the oil film thickness becomes:

$$h_1 = -\frac{6\eta_0 e^{-\beta(T_{lub}-T_0)}\alpha\overline{u_1}}{\theta\left(e^{-\alpha p_v}-e^{-\alpha p_p}\right)} \tag{13}$$

Combining the two expressions of h_1 in Eq.(10) and Eq.(13) leads to the second nonlinear equation to complete our system.

Implementation: The system of equations has been solved in Python using general nonlinear solvers. The microscale lubrication model cannot be solved without data coming from the macroscale. Namely, the strain ε, the strain rate $\dot{\varepsilon}$, the mean pressure $\bar{p}$ and the relative velocity u_1 are separately computed in the strip, here using a slab method. The roll and strip surface temperature are calculated using a 2D finite difference method [19]. The expression of p_p and p_v given in Eq.(6) and Eq.(7) are replaced in the above equations. Therefore, the equations are solved in each slab to find $\dot{\varepsilon}_a$ and Δ with an initial guess [$\dot{\varepsilon}_a > \frac{\dot{\varepsilon}}{A}$ and $\Delta > 0$]. The evolution of the area of contact A and the oil film thickness h_1 at the edge of the pit are then deduced, which closes the solution.

Results and parameters study

This section presents the numerical results of the model, and the effects of several parameters on the efficacy of MPHDL. Rolling parameters for a chosen stainless-steel grade are summarized in Table 1. A_0, L_0 and θ_0 are to be determined experimentally (see next section), however, for now, theoretical representative values will be used. Fig. 3 shows the result after one pass. The pits shrink (A increases) as the lubricant escapes and form a film at the edge, relubricating partially the plateau. The pressure at the valley increases along the bite while the plateau pressure decreases; they meet where $\Delta = 0$ at the exit of the bite region. An early cold rolling pass (initial thickness 5 mm) is selected because this is where the pit/plateau morphology of Fig. 1, hence the present model, applies.

Number of passes: Considering a schedule of reductions for three passes, $r = [18\%, 17\%, 17\%]$, Fig. 4 shows A reaches 90%, i.e. pits are almost closed after only three passes. Therefore, the MPHDL mechanism occurs only in the first passes.

Strip thickness reduction: A higher reduction rate will result in more pronounced plastic deformation of the strip. This leads to a faster flattening of the asperity thus closing of the pits. Fig. 5 shows that A evolves more with a higher reduction. Note that the length of contact (bite) changes with the reduction rate.

Pit slope: A pit with a smaller slope is easier to crush, this also leads to a higher evolution of the area of contact (Fig. 6).

Table 1 Typical rolling parameters

Parameters	**Values**
Entry strip thickness z_0	$5\ [mm]$
Lubricant temperature T_0	$40[°C]$
Lubricant viscosity μ_0	$0.08\ [Pa.s]$
Pressure viscosity coefficient α	$1.5 \times 10^{-8}\ [m^2/N]$
Roll diameter D	$60\ [mm]$
Roll speed u_r	$2.5\ [m/s]$
Temperature viscosity coefficient β	$0.08\ [°C^{-1}]$

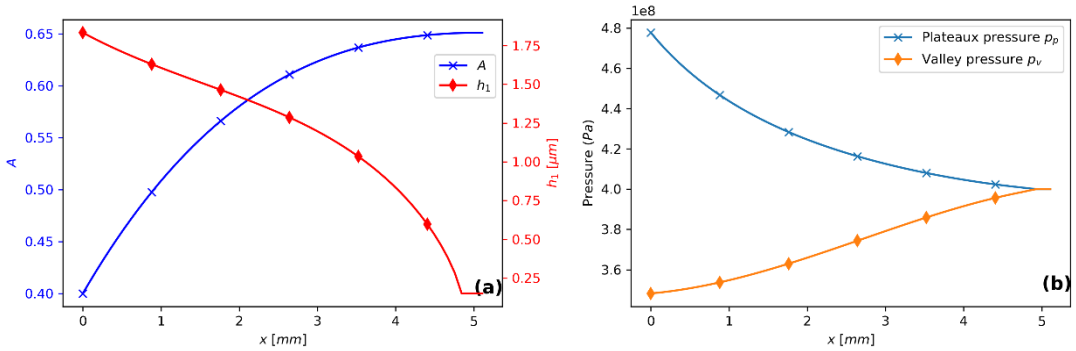

Fig. 3 (a) Variation of the contact area ratio $\boldsymbol{A}$ *and the film thickness* $\boldsymbol{h_1}$ *across the bite region ; (b) Variation of plateau and valley pressure across the bite region,* $\boldsymbol{A_0 = 0.4, L_0 = 300\ \mu m, \theta_0 = 10°}$ *and* $\boldsymbol{r = 18\%}$. $\boldsymbol{X = 0}$ *is bite inlet, bite outlet is at* $\boldsymbol{X \sim 5\ mm}$.

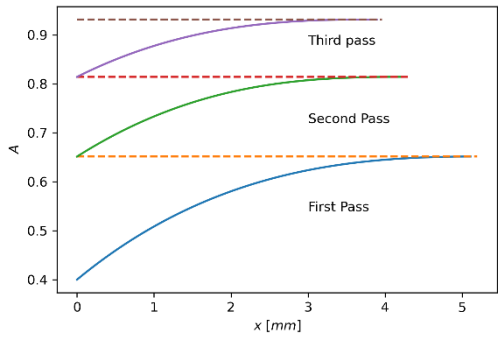

Fig. 4 Variation of area of contact $\boldsymbol{A}$ *through the bite after three passes,* $\boldsymbol{\theta_0 = 10°}$.

Lubricant viscosity and thermal effect: Lubricant viscosity plays a crucial role in the lubrication process, especially in the initial stages. Fig. 7.a shows how, as the lubricant temperature increases (Fig. 7.d), the lubricant viscosity decreases through the bite. However, it is the entry viscosity that sets the lubrication regime and the thickness of film formed by the escaping lubricant. Fig. 7.b shows that the consideration of thermal effect has an important influence on the performance of the MPHDL mechanism: the decreasing viscosity results in smaller h_1, i.e. more oil staying in the pits and delaying their crushing. Considering variations in temperature, the pit closure is decelerated by 12.5%, an effect not accounted for when this parameter is neglected. This difference in result can be even higher depending on the temperature viscosity coefficient of the lubricant as shown in Fig. 7.c ($\beta = 0$ represents the scenario where there is no thermal effect).

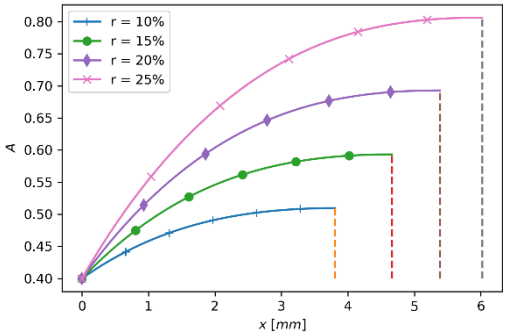

Fig. 5 Variation of area of contact $\boldsymbol{A}$ *for different reductions,* $\boldsymbol{\theta_0 = 10°}$.

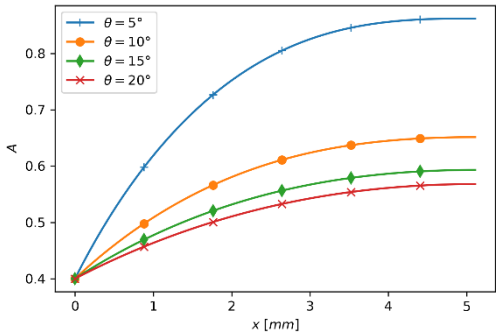

Fig. 6 Variation of area of contact $\boldsymbol{A}$ *for different pit angles* $\boldsymbol{\theta}$, $\boldsymbol{r = 18\%}$.

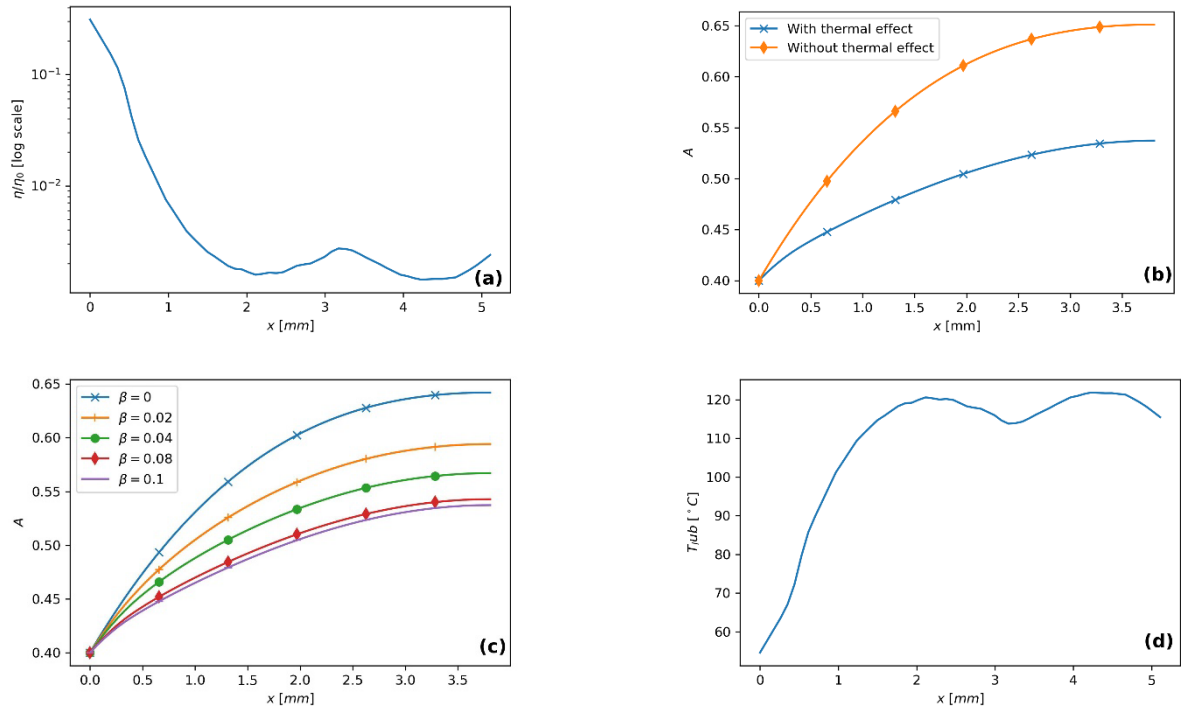

Fig. 7 (a) Variation of lubricant viscosity through the bite; (b) Effect of lubricant temperature change on the elimination of pits; (c) Effect of the temperature viscosity coefficient $\boldsymbol{\beta}$ *on the elimination of pits; (d) Lubricant temperature variation through the bite.*

Experimental validation

This section compares numerical results with experimental tests on a series of strip subjected to up to three passes of cold rolling. In both cases, the required input parameters are A_0 , L_0 and θ_0, to be found experimentally. The experiment consists in the extraction of data using a profilometer. The observation surface was chosen to be $2 \times 2\ mm$ with a pitch step of $2 \times 2\ \mu m$. The extracted file was treated and corrected using the Gwyddion software. Fig. 8 shows the result for the initial strip. The next important step is to define at which depth a feature is a pit since the assumption $\delta >> h_1$ is made in the model. To do so, a 3D height matrix (taken transverse to the rolling direction) was processed in Python to calculate the depth of features:

$$d[i,j] = H[i,j] - H_0 \tag{14}$$

Where $d[i,j]$ is the depth matrix, $h[i,j]$ the height matrix and H_0 the reference height at which a plateau is considered. In the following, H_0 is chosen, for the best representation of the surface, at a cumulative probability of 90% of the surface profile height.

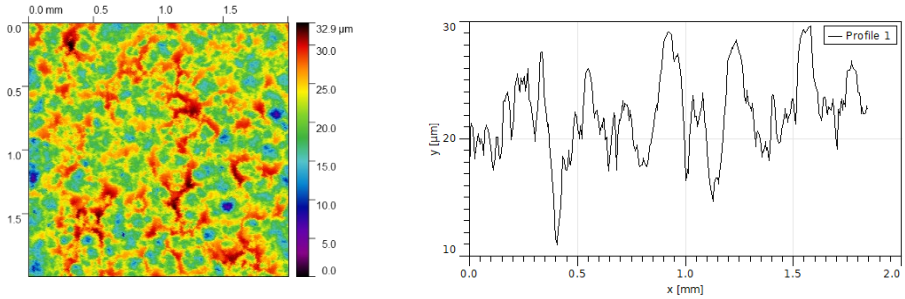

Fig. 8 Height distribution profile of the initial shot blasted strip surface.

Now, Ahmed and Sutcliffe [20] criterion can be used to identify the pits:

$$\left|\frac{d[i,j]}{R_q}\right| > \delta_p \tag{15}$$

Where $\delta_p = 1$ is the tolerance for a roll roughness of $0.4 - 0.6\ \mu m$ and Rq is the roll RMS roughness. So now, the depth of features that does not validate the criterion are set to zero in $d[i,j]$**.** Finally, A is simply the percentage of plateau ($d[i,j] = 0$) in the matrix, L is the period between two consecutive mean pits and θ is calculated through the mean depth and length of consecutive pits. The results are shown in Table 2 and Fig. 9.The results verify that the slope of asperity during the flattening process does not remain unchanged, contrary to the hypothesis in the literature models. Fig. 10 shows the numerical results agrees reasonably with the experimental data.

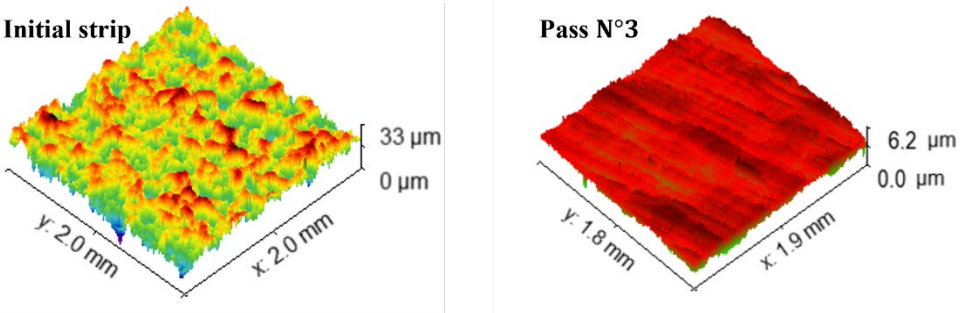

Fig. 9 3D height representation of (a) initial strip; (b) strip after three passes.

Table 2 Characterization of pit parameter

Parameters	Initial strip	First Pass	Second Pass	Third Pass
A_0	0.43	0.58	0.75	0.88
L_0	210 μm	270 μm	310 μm	380 μm
θ_0	13°	11.3°	8.5°	5°

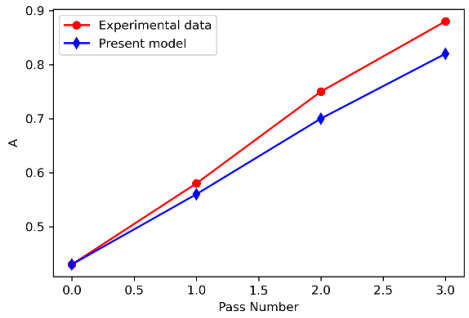

Fig. 10 Experimental Data to Numerical result comparison.

Conclusion

This paper presents a numerical model detailing the progression of oil pit closure during cold rolling through the application of the MPHDL theory. Notably, the outcomes reveal the practical suitability of this theory during the initial stages of a rolling schedule, wherein up to 90% of pits are effectively closed after three passes. A significant result of this study underscores the role of temperature variation in influencing the mechanism efficacy. The temperature impact on lubricant viscosity is identified as a key factor, introducing a nuanced perspective as it contributes to a less optimistic outcome, resulting in fewer pits being closed. Conclusively, our study enhanced its reliability by incorporating experimental data as input for the numerical model. This additional step not only validated the accuracy of our computational approach but also showed fair agreement between the numerical simulations and experimental results.

Acknowledgements

The authors gratefully acknowledge grant CIFRE 2022/1447 from ANRT, and Aperam Stainless Europe for their generous support in providing materials and data for both experimental and numerical testing, which greatly enriched the scope and outcomes of this research. We extend our gratitude for Frederic Georgi for his invaluable help and assistance in operating the profilometer.

Appendix

This Appendix presents the equations of the MPHDL model derived by Lo and Wilson [11].

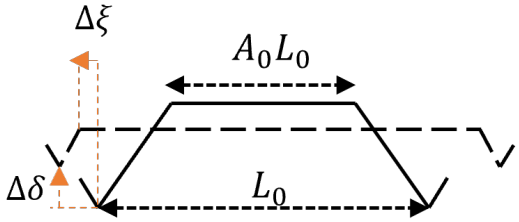

Fig. 11 Asperity flattening rate.

The current asperity spacing, contact area and mean oil velocity at the asperity edge becomes:

$$L = L_0 e^{\varepsilon} \quad \text{(A 1)}$$

$$A = A_0 e^{\varepsilon_a - \varepsilon} \quad \text{(A 2)}$$

$$\overline{u}_1 = \frac{u_1 - \frac{AL\dot{\varepsilon}_a}{2}}{2} \quad \text{(A 3)}$$

References

[1] M. Laugier, R. Boman and Y. Carretta, Micro-Plasto-Hydrodynamic Lubrication a Fundamental Mechanism in Cold Rolling, Adv. Mater. Res. 966–967 (2014) 228–241. https://doi.org/10.4028/www.scientific.net/AMR.966-967.228

[2] J. Bech, N. Bay and M. Eriksen, A Study of Mechanisms of Liquid Lubrication in Metal Forming, CIRP Ann. 47 (1998) 221–226. https://doi.org/10.1016/S0007-8506(07)62822-4.

[3] H. Kudo, M. Tsubouchi, H. Takada and K. Okamura, An Investigation into Plasto-Hydrodynamic Lubrication with a Cold Sheet Drawing Test, CIRP Ann. 31 (1982) 175–180. https://doi.org/10.1016/S0007-8506(07)63292-2

[4] J. Bech, N. Bay and M. Eriksen, Entrapment and escape of liquid lubricant in metal forming, Wear 232 (1999) 134–139. https://doi.org/10.1016/S0043-1648(99)00136-2

[5] N. Bay, J. I. Bech, J. L. Andreasen and I. Shimizu, Studies on Micro Plasto Hydrodynamic Lubrication in Metal Forming, Metal Forming Science and Practice, Elsevier, 2002, pp. 115–134. https://doi.org/10.1016/B978-008044024-8/50007-2

[6] R. Ahmed and M. P. F. Sutcliffe, An Experimental Investigation of Surface Pit Evolution During Cold-Rolling or Drawing of Stainless Steel Strip, J. Tribol. 123 (2001) 1–7. https://doi.org/10.1115/1.1327580

[7] R. Ahmed and M. P. F. Sutcliffe, Identification of surface features on cold-rolled stainless steel strip, Wear 244 (2000) 60-70. https://doi.org/10.1016/S0043-1648(00)00442-7

[8] M. P. F. Sutcliffe and F. Georgiades, Characterisation of pit geometry in cold-rolled stainless steel strip, Wear 253 (2002) 963–974. https://doi.org/10.1016/S0043-1648(02)00247-8

[9] A. Stephany, H. R. Le and M. P. F. Sutcliffe, An efficient finite element model of surface pit reduction on stainless steel in metal forming processes, J. Mater. Process. Technol. 170 (2005) 310–316. https://doi.org/10.1016/j.jmatprotec.2005.05.008

[10] Y. Carretta, J. Bech, N. Legrand, M. Laugier, J.-P. Ponthot and R. Boman, Numerical modelling of micro-plasto-hydrodynamic lubrication in plane strip drawing, Tribol. Int. 110 (2017) 378–391. https://doi.org/10.1016/j.triboint.2016.10.046

[11] S.-W. Lo and W. R. D. Wilson, A Theoretical Model of Micro-Pool Lubrication in Metal Forming, J. Tribol. 121 (1999) 731–738. https://doi.org/10.1115/1.2834129

[12] M.P.F Sutcliffe, H.R. Le and R. Ahmed, Modeling of Micro-Pit Evolution in Rolling or Strip-Drawing, J. Tribol. 123 (2001) 791-798. https://doi.org/10.1115/1.1352741

[13] W.R.D Wilson, Friction and Lubrication in Sheet Metal Forming, in: Koistinen, D.P., Wang, NM. (eds), Mechanics of Sheet Metal Forming. Springer, Boston, 1978, pp. 157-174. https://doi.org/10.1007/978-1-4613-2880-3_7

[14] D. A. Korzekwa, P. R. Dawson and W. R. D. Wilson, Surface asperity deformation during sheet forming, Int. J. Mech. Sci. 34 (1992) 521–539. https://doi.org/10.1016/0020-7403(92)90028-F

[15] D. Adeleke, D. Kalumba, L. Nolutshungu, J. Oriokot and A. Martinez, The Influence of Asperities and Surface Roughness on Geomembrane/Geotextile Interface Friction Angle, Int. J. Geosynth. Ground Eng. 7 (2021). https://doi.org/10.1007/s40891-021-00265-y

[16] W. R. D. Wilson and S. Sheu, Real area of contact and boundary friction in metal forming, Int. J. Mech. Sci. 30 (1988) 475–489. https://doi.org/10.1016/0020-7403(88)90002-1

[17] M. P. F. Sutcliffe, Flattening of Random Rough Surfaces in Metal-Forming Processes, J. Tribol. 121 (1999) 433–440. https://doi.org/10.1115/1.2834086

[18] A. Azushima, Lubrication in steel strip rolling in Japan, Tribol. Int. 20 (1987) 316–321. https://doi.org/10.1016/0301-679X(87)90059-4

[19] A. A. Tseng, A Numerical Heat Transfer Analysis of Strip Rolling, J. Heat Transf. 106 (1984) 512–517. https://doi.org/10.1115/1.3246708

[20] R. Ahmed and M. P. F. Sutcliffe, Identification of surface features on cold-rolled stainless steel strip, Wear 244 (2000) 60–70. https://doi.org/10.1016/S0043-1648(00)00442-7